From uranium(IV) oxalate to sintered UO2 : Consequences of the powders' thermal history on the microstructure

Julien Martinez, Nicolas Clavier, T. Ducasse, Adel Mesbah, F. Audubert, Bruno Corso, N. Vigier, N. Dacheux

From uranium(IV) oxalate to sintered UO_2 : consequences of the powders' thermal history on the microstructure

J. Martinez [1,2], N. Clavier [1,], T. Ducasse [1], A. Mesbah [1], F. Audubert [2], B. Corso [1], N. Vigier [3], N. Dacheux [1]*

[1] ICSM, UMR 5257 CEA/CNRS/UM/ENSCM, Site de Marcoule - Bât. 426, BP 17171, 30207 Bagnols/Cèze cedex, France

[2] CEA, DEN, DTEC/SECA/LFC, Site de Marcoule - Bât. 166 , BP 17171, 30207 Bagnols/Cèze cedex, France

[3] AREVA NC/BG Aval/DO Recyclage/RDP, Boîte à lettre 3747C-1, 1 Place Jean Millier, 92084 Paris La Défense, France

*** Corresponding author :**

Dr. Nicolas CLAVIER

ICSM – UMR 5257 CEA/CNRS/UM/ENSCM

Site de Marcoule – Bât 426

BP 17171

30207 Bagnols sur Cèze

France

Phone : + 33 4 66 33 92 08

Fax : + 33 4 66 79 76 11

nicolas.clavier@icsm.fr

Abstract :

Wet chemistry methods involving the initial precipitation of crystallized precursors are frequently reported as a promising way to prepare actinide oxides. Sintering of UO_2 powders prepared from uranium(IV) oxalate dihydrate was thus investigated in order to point out the influence of various parameters inherited from the conversion step leading from the precursor to the final oxide. In this perspective, different thermal cycles were considered, based on strictly reducing conditions, or on the successive use of oxidizing/reducing atmospheres. The modifications underwent by the samples during the conversion step were then investigated in terms of crystal structure, morphology and associated specific surface area, as well as residual carbon content. The role of these parameters in the development of sintered UO_2 microstructure was also examined, specially emphasizing the potential role of the residual carbon content over the final density.

Keywords :

Sintering / Uranium / Oxide / Oxalate / Microstructure

1. Introduction

Uranium dioxide (UO_2) as well as actinide mixed oxides such as $(U,Pu)O_2$ MOx are currently employed as fuels in several LWR-type nuclear reactors and still appear to be reference components for future concepts of Generation IV reactors, including Sodium-cooled Fast Reactor (SFR) [1]. In this framework, the sintering of these compounds has been widely investigated during the past decades [2-5]. Nevertheless, such studies frequently started from samples prepared through powder metallurgy methods and thus mainly focused their interest on parameters related to the physico-chemical characteristics of the powders (grain size, specific surface area, …) [6-8] or to the heat treatment of the pellet, *i.e.* temperature, atmosphere, …[9, 10]. Consequently, less attention was paid to the role of chemistry during the sintering process and its influence over the final microstructure of the pellets. However, the recent emergence of new ways of preparation for actinides dioxides [11-13], mainly based on the precipitation of low-temperature crystallized precursors, confers to these parameters a crucial importance for the understanding of sintering processes.

Among these precursors, and even if inorganic or metal-organic compounds were studied for long to prepare actinide oxides [14, 15], several recent studies particularly pointed out the benefits induced by the use of oxalate precursors (see for example the recent review by Abraham *et al.* and the references therein [16]). They particularly provide quick, quantitative and homogenous precipitation of cations from aqueous mixtures, and offer the possibility to incorporate simultaneously actinides presenting different oxidation states [17, 18]. Moreover, the corresponding oxides are easily obtained through a heating conversion step [19, 20]. New parameters coming from the thermal history of the oxide powder have then emerged and required to be studied. One can especially cite the crystallization state of the sample, its residual carbon content, or its morphology and reactivity, all being linked to the temperature and atmosphere of conversion.

In this study, the preparation of UO_2 powders was undertaken from $U(C_2O_4)_2{\cdot}2H_2O$ [21, 22] in order to study the influence of several precursor-related parameters over the sintering process and the subsequent pellet microstructure. In first place, the variation of the powder characteristics during the conversion step will be detailed, both at the microscopic (crystal structure, carbon content) and macroscopic (morphology, specific surface area) levels. Moreover, two different thermal cycles were considered. The first one is based on a single heat treatment under reducing atmosphere (Ar/ 5%H_2) which ensured the stabilization of the tetravalent oxidation state of uranium. Conversely, the other is composed by a first oxidizing treatment followed by a calcination at the desired temperature under reducing atmosphere.

Several authors already reported strong modifications over the powder characteristics, and their subsequent sintering capability, coming from the atmosphere used during the conversion of the precursor. As a matter of fact, White *et al.* [23] pointed out as soon as in

1981 that higher densities could be reached during the sintering of ThO_2 when using powders coming from the calcination of thorium oxalate hydrates in air rather than in reducing atmosphere. These different behaviours were mainly assigned to some differences in the carbon content within the samples, that strongly vary depending on the atmosphere of calcination [24]. Similar conclusions were further drawn for various chemical systems, including uranium-bearing mixed oxides. Along with the modification of the sintering capability of the powders, several microstructural effects were also noted. Particularly, the use of oxidizing conditions during the calcination of the precursor was found to increase the particle growth of $(U_{0.72}Ce_{0.28})O_2$ solid solutions [25]. In an opposite way, conversion under reducing conditions of thorium-uranium(IV) oxalates yielded to mixed oxide powders exhibiting high specific surface area, that could be linked to their high carbon content [26]. Moreover, heat treatments under successive oxidizing then reducing atmospheres were also successfully experimented during the sintering step of UO_2 and usually led to a significant decrease in the temperature of densification [27, 28].

The modifications underwent by the powder samples during the conversion step leading to the final oxide should then be investigated thoroughly, either at the microscopic or at the macroscopic level. More specifically, crystal structure, morphology and associated specific surface area as well as residual carbon content will be examined versus the temperature of conversion and the atmosphere chosen. The role of these parameters in the development of sintered UO_2 microstructure will be presented in a second part, specially emphasizing the potential role of the residual carbon content over the final density.

2. Experimental

2.1. Preparation of oxalate precursors

All the reagents used were of analytical-grade and supplied by Sigma-Aldrich, except uranium tetrachloride solution. The preparation of this latter was performed by dissolving uranium metal (provided by CETAMA) in hydrochloric acid. The metal pieces were first washed in 2M HCl in order to eliminate possible traces of oxide present at the surface, rinsed with water and ethanol and finally dissolved in 6M HCl. The uranium concentration of the final solution was estimated to 0.74 ± 0.02 M using the titration method developed by Dacheux *et al.* [29, 30].

Monoclinic uranium(IV) oxalate dihydrate, $U(C_2O_4)_2.2H_2O$ was further obtained through a protocol derived from that described by Clavier *et al.* [21]. Hydrochloric solution of uranium(IV) (0.3 M) was poured, without any stirring, into a large excess of oxalic acid, in order to ensure the quantitative precipitation of uranium(IV). The green precipitate rapidly formed was then separated from the supernatant by centrifugation, washed several times with deionized water then ethanol, and finally dried at 90°C in an oven.

2.2. Characterization of powders and sintered pellets

Powder X-Ray Diffraction (PXRD) diagrams were obtained by the means of a Bruker D8 diffractometer equipped with a Lynx-eye detector adopting the reflexion geometry, and using Cu $K\alpha_{1,2}$ radiation (λ = 1.54184 Å). PXRD patterns were recorded at room temperature in the $5° \leq 2\theta \leq 120°$ range, with a step size of $\Delta(2\theta) = 0.03°$ and a total counting time of about 2.5 hours per sample.

For *in situ* high temperature experiments, powders were placed in dedicated alumina boats and heated with a rate of $10°C.min^{-1}$, either under air or He/4% H_2 atmosphere. HT-PXRD patterns were recorded each 30°C from 90 to 300°C then with a step of 50°C from 300°C to 500°C, and finally each 100°C up to 1000°C. Temperature was held 15 minutes before recording the pattern in order to ensure the thermal equilibration of the sample.

All the PXRD patterns were refined by the Rietveld method using the Cox-Hastings pseudo-Voigt profile function [31] implemented in the Fullprof_suite program [32]. During all the refinements, the conventional profile/structure parameters (zero shift, unit cell parameters, scale factors, global thermal displacement and asymmetric parameters) were allowed to vary. Moreover, for each phase, modelling of the intrinsic microstructure parameters was performed by applying an anisotropic size model.

Scanning Electron Microscope (SEM) observations were directly conducted on powder samples or on sintered pellets without prior preparation such as metallization, using a FEI Quanta 200 electronic microscope, equipped either with an Everhart-Thornley Detector (ETD) or a Back-Scattered Electron Detector (BSED), in high vacuum conditions with a very low accelerating voltage (2 – 3.1 kV). These conditions were chosen in order to induce a beam deceleration effect that led to high resolution images.

In the case of powder samples, SEM observations were correlated with specific surface area measurements using adsorption/desorption of N_2 at 77K (BET method) by the means of a Micromeritics Tristar 3020 apparatus. Prior to the analyses, powder samples were outgassed at 90°C (oxalate samples) or 300°C (oxide samples) for 4 hours in order to ensure the departure of water molecules adsorbed at the surface of the solids.

For sintered pellets, the SEM observation of the microstructure was complemented by density measurements, conducted through geometrical measurements using a precision calliper. These values were further used to estimate the global porosity of the samples.

Finally, the amount of carbon in the powders was evaluated by the means of a LECO CS230 analyser, using the complete combustion of the samples in a large excess of O_2 followed by a mass spectrometer measurement of CO_2. In order to get quantitative values, a blank and a series of standards (steels containing 0.182 to 3.10 wt.% of carbon) were analysed prior our samples.

2.3. Thermal analyses and sintering

Thermogravimetric analyses were undertaken thanks to a Setaram Setsys Evolution equipped either with a type-S thermocouple (Pt / Pt-10%Rh) when working in air or with W5 device (W-5%Re / W-26%Re) for analyses performed under reducing atmosphere. After recording of a baseline using an empty crucible (100 µL), weight loss was monitored during a heat treatment up to 1000°C with a rate of 10°C.min^{-1}. Moreover, the gaseous species emitted during the heat treatment were analysed by the means of Hiden Analytical QGA analyser using mass spectrometry.

Following the characterization of the UO_2 samples versus the temperature of conversion from oxalate precursors, several experiments were dedicated to the sintering of the powders synthesized. For this purpose, green pellets of 5 mm diameter and about 1 to 2 mm width were prepared by uniaxial pressing (500 MPa) in a tungsten carbide die. First, dilatometric study allowed us to precise the temperature corresponding to the densification of the samples. These measurements were conducted on a Setaram Setsys Evolution apparatus. In this case, heat treatments were systematically undertaken under Ar/2% H_2 flux up to

1600°C with a rate of 10°C.min^{-1}. Dwell time of 30 minutes was then considered before sample was cooled down to room temperature at 30°C.min^{-1}.

In a second step, the microstructure of the pellets obtained after a heat treatment at 1550°C (8 hours – Ar/ 5%H_2) was investigated, mainly in terms of density and grain size.

3. Results and discussion

3.1. Conversion of the precursors

In order to point out the role of the atmosphere during the conversion of uranium oxalate toward the physico-chemical properties of the resulting oxide powder, two different thermal cycles were considered. The first one was conducted under reducing Ar/2% H_2 atmosphere at various temperatures ranging from 200 to 1000°C, thus ensuring the stabilization of the tetravalent oxidation state of uranium. The sample was then heated up, considering a rate of 200°C.hour^{-1}, then maintained at the desired temperature for 4 hours. On the other hand, a two-step procedure was also tested, composed by a first calcination under air for 4 hours at a given temperature in the 200-1000°C range, followed by a reducing heat treatment (Ar/ 2% H_2) for 4 hours at the same temperature.

3.1.1. Thermogravimetric analyses

TG analyses were first performed in order to evidence the reaction scheme driving the decomposition of uranium(IV) oxalate dihydrate under the different atmospheres chosen (Figure 1). Moreover, the experimental setup was implemented with a mass spectrometer in order to analyse the gases emitted during these processes. The thermogravimetric curve recorded under reducing Ar/H_2 atmosphere presents the characteristic steps already reported in the literature for the decomposition of An(IV) oxalate dihydrate (An = Th [33] and/or U [34, 35]). The first one, occurring between 100 and 200°C corresponds to the loss of one water molecule, leading to the uranium(IV) oxalate monohydrate. Similarly, the loss of additional 5% between 200 and 250°C, was assigned to the complete dehydration of the sample, as attested by the detection of water vapour through mass spectrometry. Finally, the decomposition of oxalate species, correlated to the emission of gaseous CO and CO_2 was found to take place mainly between 300 and 400°C. Despite this decomposition, a residual weight loss was still recorded up to 600°C and could indicate the presence of amorphous carbonate species in the 400-600°C range.

The three steps detailed above were also observed when heating uranium(IV) oxalate dihydrate in air. Nevertheless, if the dehydration step still occurred in the same range of temperature, the decomposition of oxalate species was found to take place at lower temperature as it ended below 350°C. Such difference could be ascribed to the more efficient elimination of the carbon species in air. Indeed, in such conditions, CO coming from the decomposition of C_2O_4 species is mainly oxidized by O_2 while it tends to disproportionate under inert or reducing atmosphere to form CO_2 and elemental carbon (Boudouard equilibrium) [36]. Moreover, an additional weight loss was pointed out at around 650°C and

could be ascribed to the transformation of an intermediate uranium carbonate or oxocarbonate into the final oxide product, probably as U_3O_8.

(a)

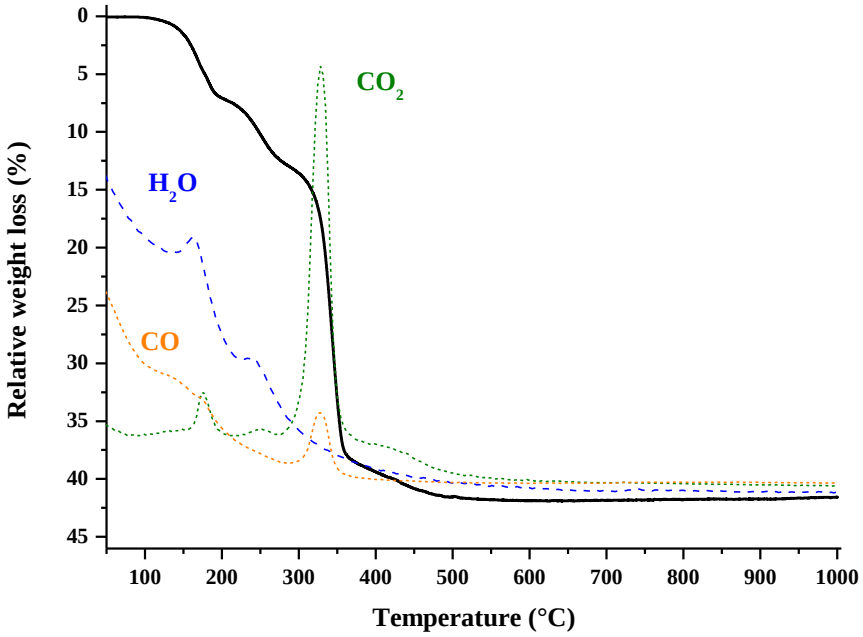

(b)

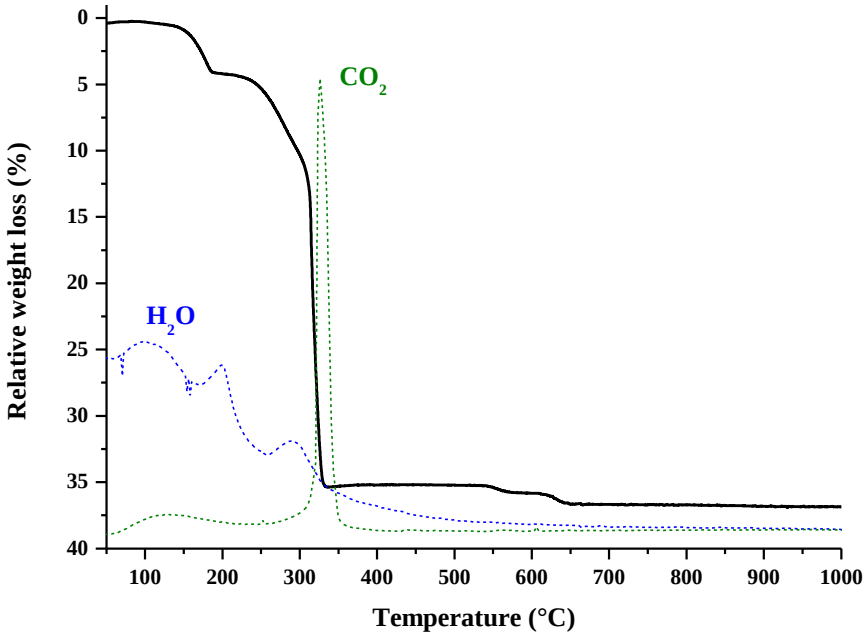

Figure 1. TGA-MS curves recorded during the decomposition of $U(C_2O_4)_2$. $2H_2O$ under Ar/H_2 (a) or in air (b) atmosphere.

3.1.2. Variation of carbon content

Consequently to the TG analyses, the residual carbon content of the UO_2 powders obtained from the conversion of oxalate precursor through the two thermal cycles considered was analysed. Indeed, even if the literature concerning the effect of residual carbon on the sintering of oxide ceramics is extremely scarce, such parameter is still frequently considered from an industrial point of view as carbon species could remain from numerous processes, including debonding steps aiming to eliminate binders and/or pore formers [37].

Whatever the atmosphere chosen, and as expected from the decomposition of oxalate entities evidenced through TGA, the amount of carbon in the samples systematically dropped down below 0.8 wt.% above 300°C (Figure 2). Such amount would correspond to less than 3.8 wt.% of CO_3 entities, which appears to be in very good agreement with the recent values reported by Tyrpekl *et al.* during the study of uranium(IV) and thorium(IV) nanograined oxalates (*i.e.* < 3.4 wt.% of carbonate) [38]. Nevertheless, the heat treatments combining the use of oxidizing and reducing atmospheres appeared to be much more efficient to operate the carbon elimination. Again, this observation could be correlated with the Boudouard equilibrium that led to the disproportionation of CO into C and CO_2 under inert atmosphere [36]. In these conditions, the amount of carbon still remaining in the samples heated in reducing atmosphere was systematically found to be 4 to 5 times higher than that measured in samples previously calcined in air. Also, the nature of the carbon species inside the oxide phase and their localisation could be widely different. On the one hand, several authors reported the presence of carbonated or oxocarbonated species when converting actinide oxalates under inert or reducing atmospheres [20]. Such compounds could still exist in some of the samples fired at the lowest temperatures (typically below 600°C), and are expected to delay and/or hinder the sintering processes [39]. However, the residual carbon content is more likely to be present in an amorphous state as the formation of defined oxycarbide species could be excluded considering the carbon amount in the samples (typically less than 10 wt.%) [40]. On the other hand, it is most likely that the carbon present in the samples initially heated in air remained as elemental and amorphous carbon, that could be located either in solid defects (such as boundaries between crystallites) or directly inserted in the fluorite-type lattice of UO_2. Indeed, the presence of carbonates intermediates during the oxalate-conversion was ruled out by several authors when working under oxidizing atmosphere and/or with high values of heating rates [35, 41].

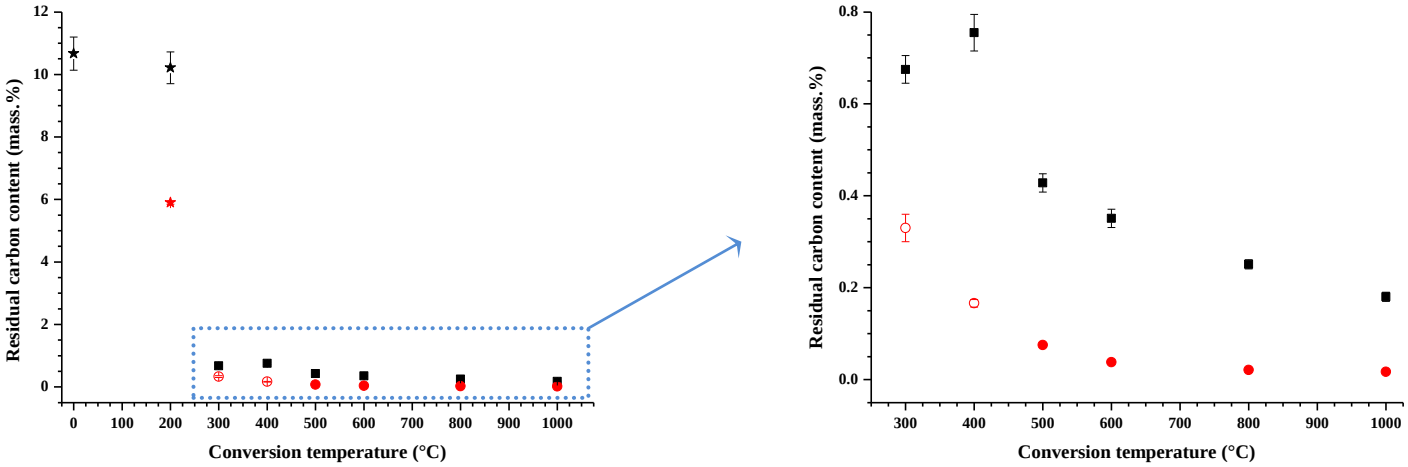

Figure 2. Variation of the residual carbon content in the precursor after the conversion of $U(C_2O_4)_2$. $2H_2O$ through reducing (black) and oxidizing/reducing (red) thermal cycles. Stars correspond to oxalate samples, open symbols to a mixture of uranium oxides and full symbols stand for UO_2 powders.

3.1.3. HT-PXRD

The samples were further examined *in situ* during both thermal cycles by the means of HT-PXRD. The patterns collected when heating under reducing atmosphere are first gathered in Figure 3. Data initially recorded at room temperature confirmed the formation of uranium(IV) oxalate dihydrate during the initial precipitation step. Indeed, the unit cell parameters of $U(C_2O_4)_2$. $2H_2O$ (monoclinic structure, space group C2/c) were estimated to a = 10.5174(5) Å, b = 8.7085(6) Å, c = 9.2433(7) Å and β = 90.398(3)° Å through Rietveld refinement and agreed well with the values reported in the literature [21]. The characteristic PXRD lines of this compound were then conserved up to 60°C: even if a phase transition toward an orthorhombic variety was reported around 40°C [21], the conditions of acquisition used for HT measurements hinder the detection of the slight pattern modifications associated. From 90°C, the appearance of additional peaks marked the progressive dehydration of the initial compound, first leading to $U(C_2O_4)_2$. H_2O (see red patterns on Figure 3) then to anhydrous $U(C_2O_4)_2$ (orange patterns). These latter were unambiguously identified by analogy with the homologous thorium based compounds, namely $Th(C_2O_4)_2$. H_2O and $Th(C_2O_4)_2$ [33].

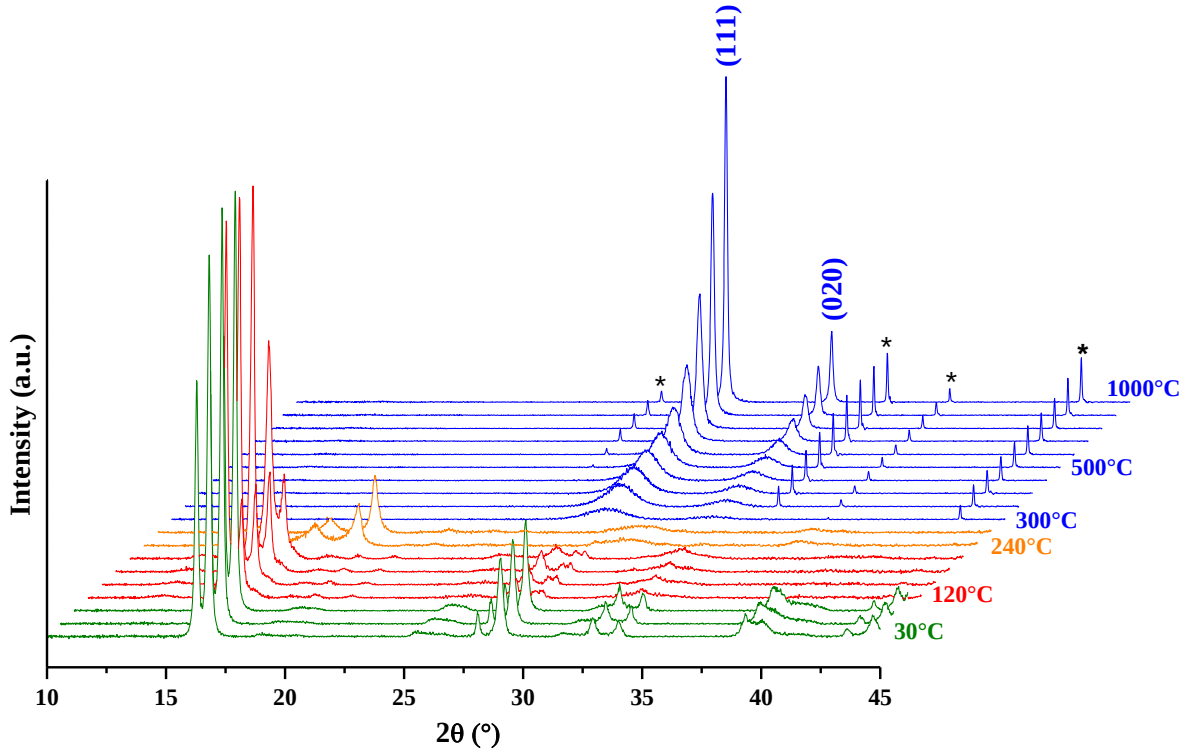

Figure 3. HT-PXRD analysis of $U(C_2O_4)_2$. $2H_2O$ under reducing He/4% H_2 atmosphere. Diffraction planes are indicated for the main reflections of the fluorite structure while stars point out the PXRD lines of the sample holder.

Above 270°C, the intensity of the PXRD lines decreased strongly, indicating the progressive amorphization of the sample associated to the decomposition of oxalate entities leading to the oxide, as evidenced during the TG analyses. Indeed, the characteristic pattern of the Fm-3m fluorite-type structure of UO_2 [42] was detected as soon as 300°C, even if the wide peaks collected evidenced the poorly crystallized and/or the nanosized nature of the sample. The increase of temperature up to 1000°C was then correlated with the narrowing of the PXRD lines thus to the growth of the coherent domains. As a matter of fact, Rietveld refinement revealed an increase in the average coherent domains size from 3 nm at 300°C to about 60 nm at 1000°C (Figure 4). Finally, the refinement of the PXRD pattern recorded after cooling the sample down to room temperature led to a value of the unit cell parameter of a = 5.467(1) Å, in good agreement with that usually reported for nearly stoichiometric UO_2 (a = 5.471 Å, V = 163.76 $Å^3$) [42].

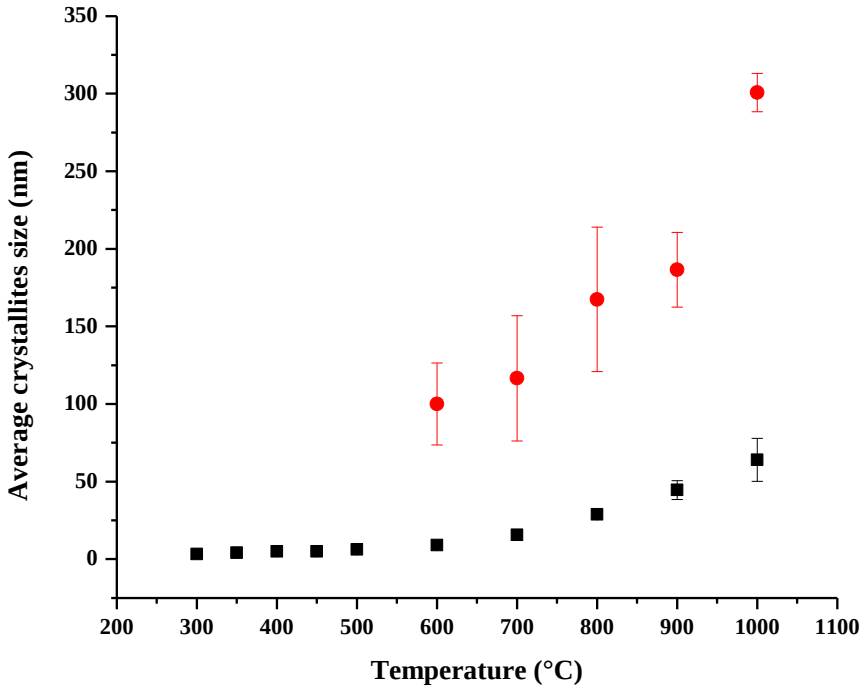

Figure 4. Variation of the average crystallites size in UO_2 coming the conversion of $U(C_2O_4).2H_2O$ through reducing (■) and oxidizing/reducing (●) thermal cycles.

Additionally, the results obtained with the second thermal cycle clearly evidenced the impact of the oxidizing atmosphere on the behaviour of uranium(IV) oxalate dihydrate. Even if the dehydration of $U(C_2O_4)_2.2H_2O$ first followed the same trend than in reducing atmosphere between room temperature and 100°C, noticeable changes occurred above this latter temperature (Figure 5). The amorphization resulting from the decomposition of oxalate entities appeared to take place at much lower temperature than in reducing temperature, starting approximately from 150°C. Such decrease of the decomposition temperature could arise both from the early oxidation of uranium(IV) into uranium(VI) but also from the more efficient elimination of carbon species in air. Such behaviour was also stated from TG analyses although the decomposition of oxalate groups was supposed to occur at higher temperature (i.e. at about 300°C). The difference between the two techniques could thus arise from the time needed to record the XRD pattern that led to different heating time at each temperature. Finally, starting from 300°C, the amorphous compound turned into the hexagonal variety of α-U_3O_8 (space group $P\bar{6}2m$) [43], thus confirming the oxidation of U(IV). This oxide was found to be stable up to 900°C under the conditions used then started to turn into the orthorhombic β-U_3O_8 (space group Cmcm) [44, 45].

After cooling the sample down to room temperature, similar measurement was conducted under reducing atmosphere without any intervention on the sample. In these conditions, the shrinkage of the powder associated to its calcination led us to observe systematically the characteristic PXRD lines of the sample holder. Despite of this bias, the PXRD pattern recorded at room temperature confirmed the preparation of U_3O_8 after heating in air. This latter appeared to be stable up to 500°C then tended to reduce to finally form the fluorite-type UO_2 above 550°C. As observed when firing the oxalate precursor under inert atmosphere, the increase of the temperature mainly led the peaks to narrow, thus indicating a growth of the coherent domains (i.e. crystallite size). Nevertheless, the average crystallite size appeared to be widely higher when using oxidizing/reducing heat treatment (Figure 4). As instance, it reaches more than 300 nm after firing the sample at 1000°C under the latter conditions, while it was only about 60 nm when using strictly reducing atmosphere. Even if the influence of the heat treatment duration (which increases from 4 to 8 hours when applying successively oxidizing/reducing conditions) cannot be ruled out completely, such difference originates from the oxidization of uranium in air that is frequently associated to an acceleration in the grain growth kinetics [46]. Indeed, uranium diffusion in orthorhombic U_3O_8 proceeds at rates much faster than in UO_2 [47], with D_U values comparable to that determined in super-stoichiometric $UO_{2.22}$. Such difference in the diffusion coefficients could be as high as 3 orders of magnitude when comparing log D_U at 1500°C for UO_2 and $UO_{2.2}$ [48].

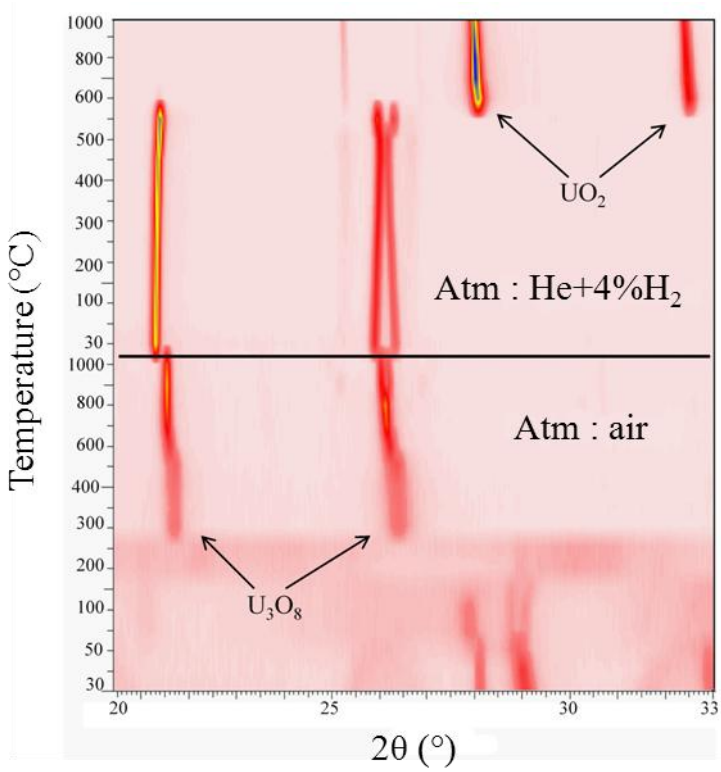

Figure 5. HT-PXRD analysis of $U(C_2O_4)$. $2H_2O$ under oxidizing (air) then reducing (He/4% H_2) atmosphere.

Another difference generated by the modification of the firing atmosphere can be noted when comparing the lattice parameters of UO_2 determined from *in situ* HT-PXRD measurements (Table 1). Indeed, for heating temperatures ranging from 600°C to 1000°C, the unit cell volumes refined for compounds prepared under reducing conditions appeared to be systematically higher than those evaluated for samples fired through the oxidizing/reducing cycle. Although this small difference only reflected a slight swelling of the lattice (typically below 0.5%), it could be assigned to the presence of residual carbon species within the UO_2 samples, even if the chemical form as well as the precise location of this carbon content remained widely unknown.

However, one can note that the difference in the lattice volume is negligible at 600°C. At this temperature, thermogravimetric analysis revealed that oxalate decomposition might be unachieved under reducing atmosphere, thus that carbonated species could remain in the solid. Based on steric considerations, such species are more likely located outside of the oxide lattice, for example in grain boundaries. On the other hand, the residual carbon content remaining in the samples heated above 700°C should be mainly composed of amorphous carbon that can be inserted directly within the UO_2 lattice, for example as interstitial defects. The presence of carbon incorporated as punctual defects could then be correlated to the swelling observed in the UO_2 lattice. Moreover, this swelling was found to decrease with the conversion temperature, which could be directly correlated to the diminution of the carbon content in the samples previously evidenced. In these conditions, once the UO_2 sample finally obtained at 1000°C was cooled down, the refinement of the unit cell parameter led to $V = 163.5(1)$ Å^3, thus did not differ significantly from that obtained for the sample heated under reducing conditions.

Table 1. Variation of the unit cell volume of UO_2 versus temperature during the conversion of $U(C_2O_4)_2$. $2H_2O$ under reducing or oxidizing then reducing atmosphere.

Temperature (°C)		600	700	800	900	1000	Back RT
Cell volume (Å^3)	Ar/H_2	166.53(3)	167.37(2)	167.95(2)	168.4(1)	169.10(2)	163.36(2)
	Air + Ar/H_2	166.45(5)	166.74(4)	167.38(6)	168.1(2)	168.7(2)	163.5(1)
Swelling (%)		N.S.	0.40	0.30	0.10	0.20	N.S.

N.S. : not significant

Finally, the nature of the powders obtained from the thermal cycle combining the use of oxidizing then reducing atmosphere for the conversion of oxalate precursor was checked through PXRD measurements conducted at room temperature. The patterns recorded, presented as supplementary material (Figure 6), evidenced that pure UO_2 was only obtained for conversion temperatures starting from 500°C. Indeed, the sample prepared after heating at 400 °C turned out to be composed of a mixture of UO_2 and β-U_3O_8 while lower temperatures did not allow the complete decomposition of the oxalate precursor.

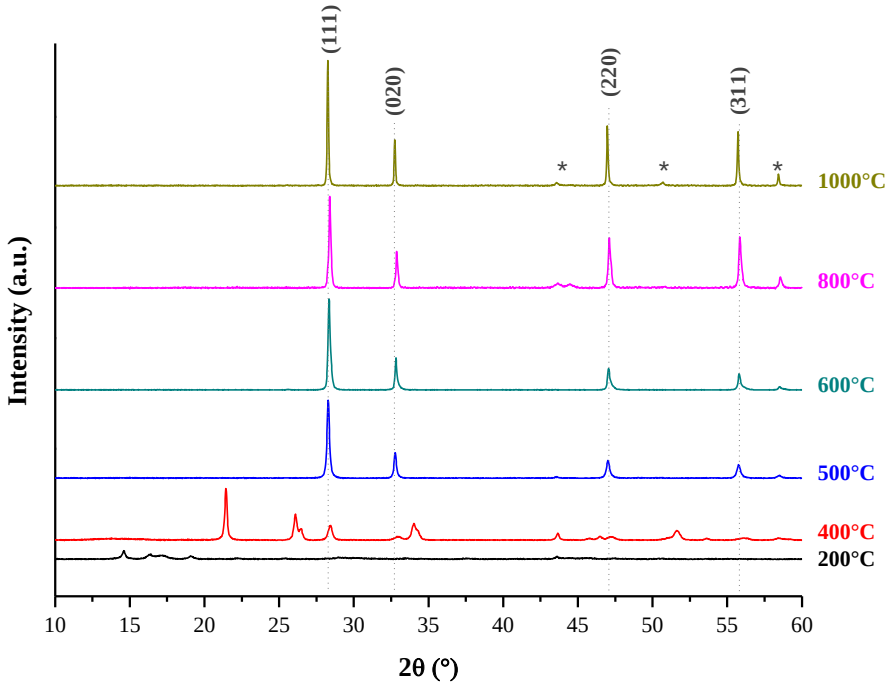

Figure 6. XRD patterns recorded after the conversion of $U(C_2O_4).2H_2O$ through oxidizing/reducing thermal cycles performed at various temperatures. Diffraction planes are indicated for the main reflections of the fluorite structure while stars point out the PXRD lines of the sample holder.

3.1.2. SEM Observations

In order to complete the data obtained by the means of HT-PXRD, the morphology of the powders prepared by firing uranium(IV) oxalate dihydrate through the two thermal cycles considered was also investigated by the means of SEM observations and specific surface area measurements using N_2 adsorption/desorption (BET method).

The SEM micrograph of the starting oxalate precursor (Figure 7) exhibited the well-known shape of $An^{(IV)}(C_2O_4)_2.2H_2O$ samples, characterized by square platelets of about 2 µm in length, themselves composed by smaller submicrometric crystallites [35]. The conversion

of the powder sample under reducing atmosphere did not induce any significant modification of the general morphology of these platelet aggregates up to 1000°C, although a drastic decrease of their average grain size was noted and evaluated to about 50% in length. This phenomenon arose both from the decomposition of the oxalate species between 300 and 500°C and from the growth of the crystallites at higher temperatures leading to the densification of the aggregates [13].

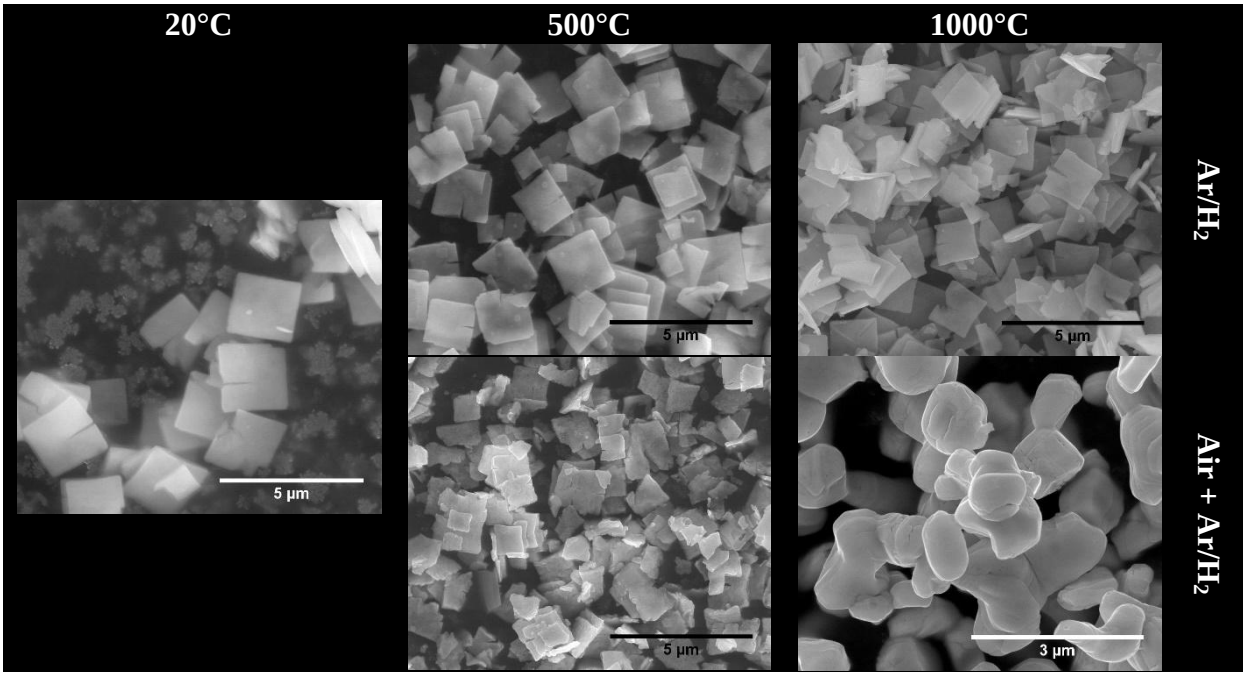

Figure 7. SEM observations of $U(C_2O_4)_2$. $2H_2O$ and of the oxide powders obtained after heating treatment at 500°C and 1000°C following the two thermal cycles considered.

On the other hand, the succession of oxidizing then reducing heat treatments appeared to have a greater impact toward the morphology of the powders. If the micrograph recorded after heating at 500°C still revealed square platelets, these latter were found to present a large quantity of surface defects including cracks. This difference was even more obvious when observing the sample fired at 1000°C, for which the morphology was completely modified. In these conditions, the powder appeared to be composed by barely spherical grains of about 1 to 2 µm in diameter that already started to sinter, as evidenced by the presence of grain boundaries on the SEM micrograph. Such modifications were be correlated to the oxidization of UO_2 into U_3O_8 during the first step of the heat treatment, which was already reported to be accompanied by an increase in the grain growth kinetics [46]. It could then be assumed that the changes occurring at the molecular level also led to drastic variation in some macroscopic parameters such as morphology. Several authors already described an exaggerated grain growth along with the concomitant spheroidization of the grains during the oxidizing sintering

of UO_2 [46] or sintering of mixture of UO_2 and U_3O_8 [49], that are referred as "solarization" phenomenon [50, 51]. Although such behaviour was mainly pointed out in compacts, it is also likely to happen in powder samples at high temperature, thus explaining the change in the morphology observed in our samples above 500°C.

These significant changes in the powder morphology were also noticed from the measurement of the associated specific surface area (Figure 8). However, the trend observed in the variation of the S_{SA} value was found to be very similar between room temperature and 300°C, and characterized by a strong increase from about 1 to 5-6 $m^2.g^{-1}$. Such behaviour was systematically observed during the decomposition of metal oxalates [19] and was assigned to the development of mesopores due to the elimination of carbonated gaseous species (i.e. mainly CO and CO_2) [52, 53]. In a second step, the heat treatment under reducing atmosphere was correlated to a sharp decrease of the specific surface area above 300°C, linked with the elimination of mesoporosity thanks to crystallite growth. Even if such process should have occurred during the thermal cycle in oxidizing/reducing conditions, it was also accompanied by the formation of multiple surface defects (pores, cracks), then by a complete change of the powder morphology, as evidenced by SEM observations. A decrease in the S_{SA} value was then still observed but appeared much lower than in the first case described, with values systematically above 3 $m^2.g^{-1}$.

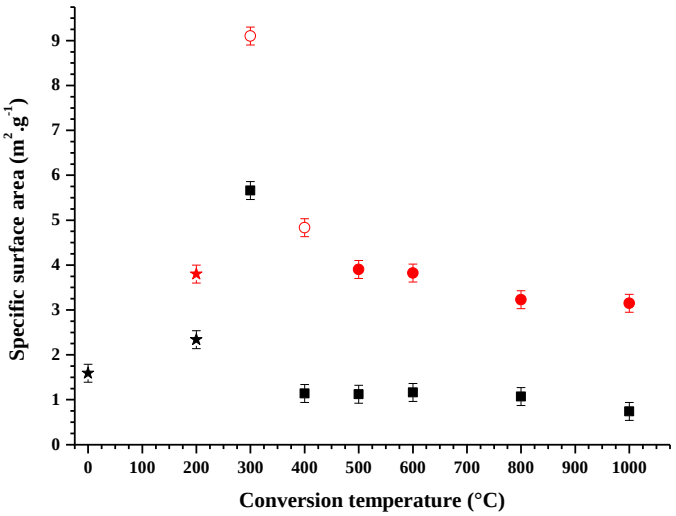

Figure 8. Variation of the precursors' specific surface area after the conversion of $U(C_2O_4)_2.2H_2O$ through reducing (black) and oxidizing/reducing (red) thermal cycles. Stars correspond to oxalate samples, open symbols to a mixture of uranium oxides and full symbols stand for UO_2 powders.

3.2. Sintering

3.2.1. Dilatometric study

Uranium oxide samples coming from the conversion of the oxalate precursors following the two different thermal cycles considered were both analysed through dilatometric study. Figure 9a presents the relative linear shrinkage measured when heating UO_2 powders obtained by conversion up to 1600°C under reducing conditions at three different temperatures. In this case, the general trend of the dilatometric curve appeared to differ strongly depending on the temperature of conversion considered. Indeed, the powder prepared after heating uranium(IV) oxalate dihydrate at 500°C presented three distinct steps of shrinkage : the first one lied between 500 and 700°C, the second from 900 to 1400°C while the last step took place above 1400°C. In order to get a better understanding of the different phenomena occurring during the shrinkage of the pellet, additional measurement was conducted by coupling dilatometry with mass spectrometry (Figure 9b). The analysis of the gases emitted evidenced that the first step of shrinkage is due to the combination of grain growth and densification phenomena, along with the elimination of important amounts of carbon that came from the incomplete decomposition of the oxalate precursor at 500°C and/or the residual existence of carbonated or oxocarbonated entities. Conversely, no other gas emission was recorded above 600°C, showing that the two additional shrinkage steps were due to sintering. On this basis, the first one (800-1200°C) could be correlated to densification and grain growth phenomena occurring within the square agglomerates, while the final stage probably corresponds to sintering between the agglomerates [54].

The curve obtained from the powder prepared by heating $U(C_2O_4)_2.\ 2H_2O$ at 800°C appeared to present only two shrinkage steps. As the temperature used for the conversion certainly allowed to fully decompose oxalate groups, no shrinkage was recorded between room temperature and 800°C. Above this temperature, the steps previously described and assigned to the sintering inside then between the agglomerates were observed. Moreover, it is important to note that both onset temperatures and shrinkage rates associated with these phenomena remained almost unchanged when modifying the temperature of conversion.

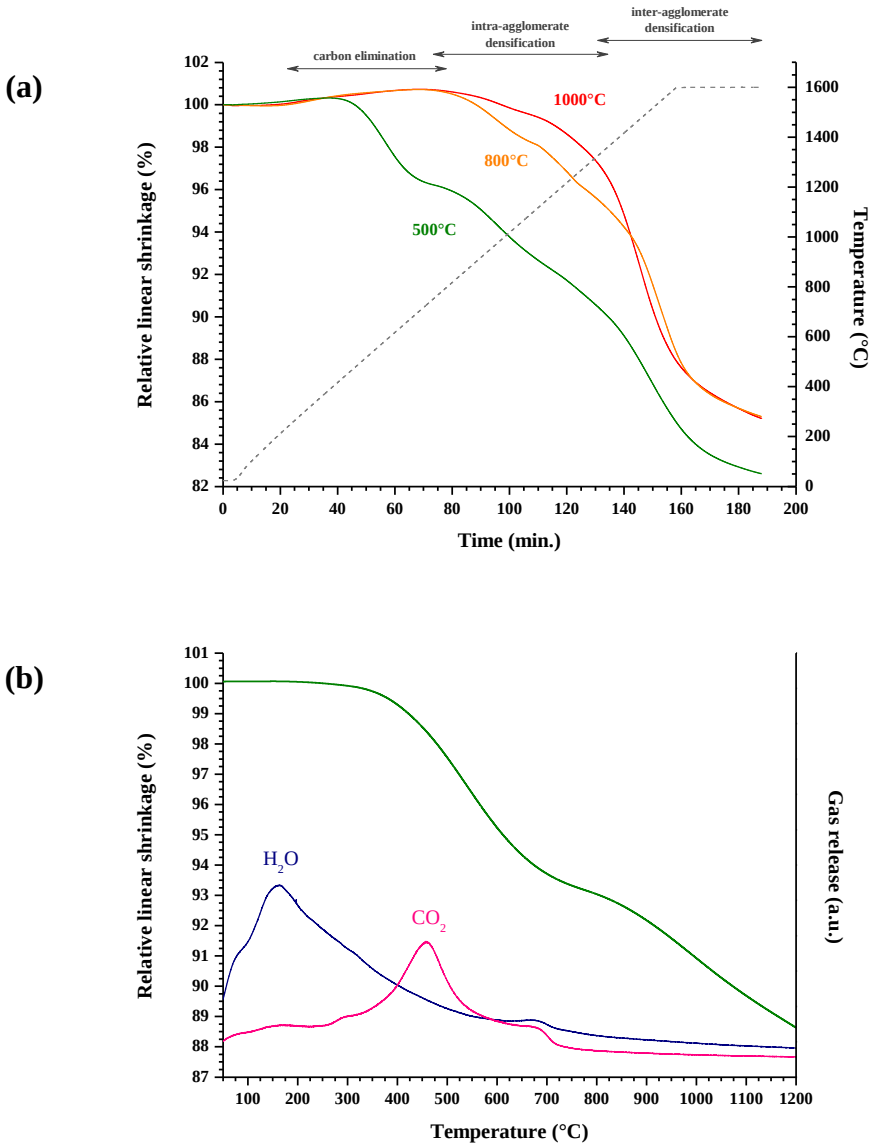

Figure 9. Dilatometric study of the samples obtained after conversion of $U(C_2O_4)_2$. $2H_2O$ under reducing atmosphere (a) and dilatometry/MS measurement from the sample heated at 500°C (b).

The last curve obtained from the powder prepared at 1000°C exhibited a similar behaviour than that described above. Nevertheless, the step ascribed to the sintering within the agglomerates (here occurring between 850°C and 1200°C) appeared to be much more limited as it accounted only for 2% of linear shrinkage. On this basis, the densification of the agglomerates probably mainly took place during the conversion of the oxalate precursor. Thereafter, the major part of the shrinkage was observed starting from 1200°C and corresponded to the densification of the pellet, *i.e.* to the sintering between the agglomerates. Once again, despite the difference existing between the starting powders, the shrinkage rate associated to the pellet densification did not appear to be significantly modified. On this basis, the sintering temperature of the three powders studied was found to occur maily above

1600°C, which fits well with the results reported in the literature for the densification of UO_2 in reducing atmosphere [9].

Dilatometric data were then collected from the powders converted under oxidizing then reducing conditions. They were found to be much simpler and systematically presented only one shrinkage step (Figure 10). This latter was thus correlated to the sintering of the pellet. Nevertheless, and conversely to the previous case, both the onset temperature and the shrinkage rate appeared to depend strongly on the conversion temperature considered. In these conditions, the highest shrinkage rate was obtained at about 1300°C from the powder converted at the lowest temperature (*i.e.* 500°C) and at 1600°C for the powder initially heated at 1000°C.

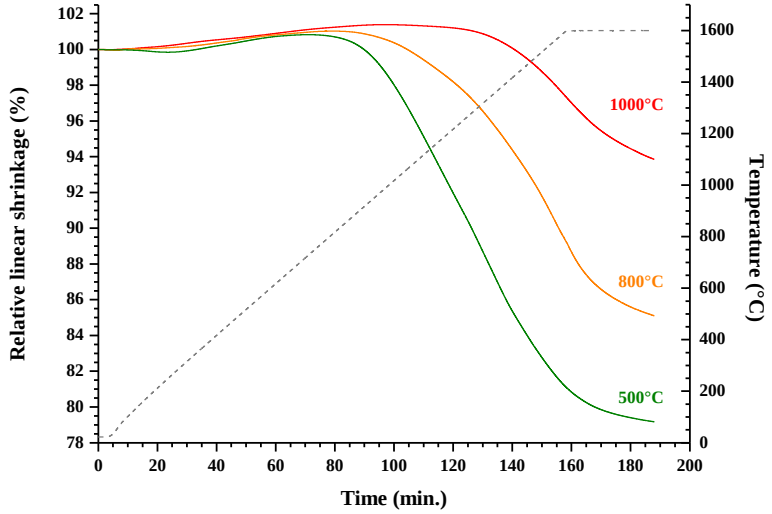

Figure 10. Dilatometric study of the samples obtained after conversion of $U(C_2O_4)_2.2H_2O$ under oxidizing then reducing atmosphere

This difference originates from the variability of the reactivity of the starting powder versus the temperature of conversion, even if the specific surface area of the samples did not undergo significant modifications. Indeed, the important increase of the coherent domain length (i.e. crystallite size) could significantly modify the sintering ability of the powder as it is likely to slow the diffusion processes. As an example, the sintering of single crystals of zirconia was already reported to occur more slowly than that of polycrystalline powders of the same size, as the presence of boundaries between the crystallites acts as preferential diffusion paths [55]. Similarly, the sintering of $(U,Ce)O_2$ solid solutions was recently found to take place at lower temperature when starting from nanocrystalline powders [56]. Also, the significantly lower temperature of sintering obtained with the powder converted at 500°C could come from the difference of morphology stated from SEM observations. Particularly,

the presence of macroscopic defects in the powder, such as cracks, could favour the rearrangement of the particles during the shaping step, leading to higher values for green density. In these conditions, the powder composed by square platelets aggregates appeared to be most favourable to sintering, even if such oriented morphology could also led to several drawbacks, especially when looking at the mechanical properties of the pellets.

3.2.2. Microstructural evaluation

Finally, the microstructure of the pellets sintered from the various oxide powders detailed previously was investigated. For that purpose, sintering operating conditions were set to a heat treatment of 8 hours at 1550°C under Ar/H_2 atmosphere. In these conditions, the variation of the geometrical density of the compact bodies versus the conversion temperature of the precursor appeared to vary oppositely depending on the atmosphere chosen when firing oxalate compounds (Figure 11). Indeed, for oxide powders prepared by heating uranium(IV) oxalate dihydrate under reducing atmosphere, the relative density increased moderately from 86% to 89% of the calculated value. Such weak variation was found to be in good agreement with the conservation of the powder morphology during the conversion, which probably did not affect strongly the reactivity of the powder. More surprisingly, the influence of the remaining carbon species, either present as carbonates or as elemental carbon in the structure, also appeared to be rather limited even if their amount showed important variations throughout the heat treatment of the precursors. On this basis, the elimination of carbon is probably pursued and completed during the sintering heat treatment before the closure of the open porosity, *i.e.* before or at the beginning of the isotherm dwell. In these conditions, the elimination of gaseous CO and/or CO_2 should not lead to the formation of additional porosity. Conversely, as it was stated previously, the part of residual carbon that cannot be removed under reducing conditions, even after annealing at high temperature, probably hinder the diffusion processes in the samples and delay the densification [37] which accounts for the rather low relative densities determined, that remained systematically below 90% of the calculated value.

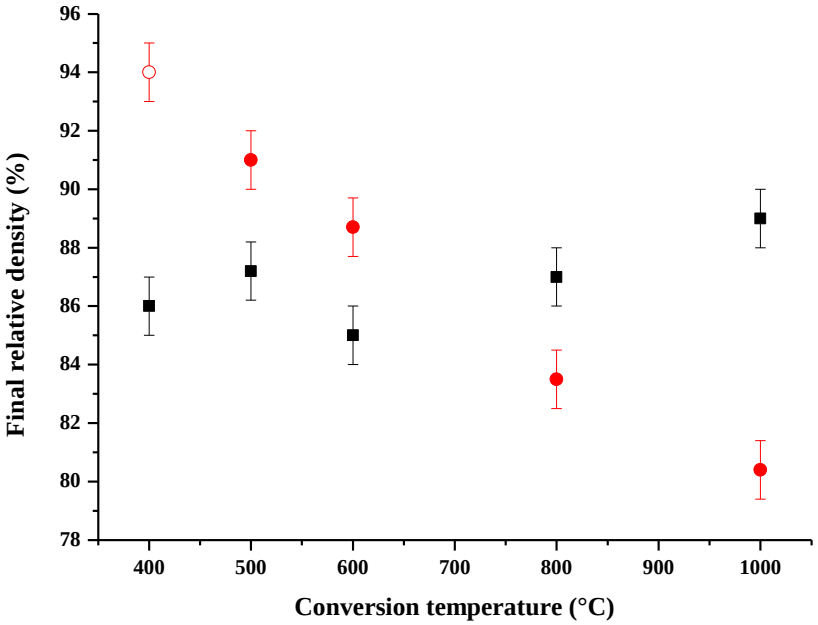

Figure 11. Variation of the final relative density of sintered UO_2 pellets (T = 1550°C, t = 8 hours) prepared from converted $U(C_2O_4)_2$. $2H_2O$ through reducing (■) and oxidizing/reducing (●) thermal cycles. Open symbol corresponds to the starting powder composed of a mixture of UO_2 and U_3O_8 while full symbols stand for UO_2 powders.

In an opposite way, the relative density of the pellets prepared from powders converted successively in oxidizing then reducing atmosphere was found to decrease as a function of the conversion temperature. Indeed, the highest final density was obtained for the powder prepared at the lowest temperature, i.e. 400°C. Nevertheless, in these conditions, the starting compound was composed of a mixture of UO_2 and U_3O_8, which was frequently reported to lead to dense pellets through reducing sintering [9]. The decrease observed in the final densities of the pellets prepared from powders converted above 400°C could then be assigned to two distinct phenomena. First, and as it was stated before, the reduction of U_3O_8 into UO_2 during the heat treatment led to the decrease of diffusion coefficient of uranium in the solid, thus to a slowdown in the sintering kinetics. Also, the modification in the grains morphology and the concomitant crystallite growth was found to decrease the reactivity of the powders. Once again, the effect of the remaining carbon species did not appear to be predominant, as the more efficient elimination of carbon provided by oxidizing/reducing conversion was found to be widely overtaken by the morphological modification underwent by the powder.

In parallel, the SEM observations performed on selected samples (Figure 12) confirmed the conclusions drawn from the density measurements. On the one hand, the open

porosity observable at the surface of the pellets prepared from powder converted under Ar/H_2 atmosphere was found to drop down when increasing the temperature of conversion. In the same time, the size and location of such pores was strongly modified. Indeed, the samples sintered from powders converted at 500°C and 800°C mainly presented intergranular pores of about 1 µm in diameter while that obtained from the sample initially fired at 1000°C only revealed very small open pores (approximately of 100 nm), all located inside the grains. Conversely to the porosity, the average grain size did not vary significantly with the starting powder and was found to be systematically in the range of 1 to 2 µm.

On the other hand, as it was stated previously, the samples prepared through oxidizing/reducing conversion led to an opposite behaviour during sintering. Indeed, the pellet obtained from the powder converted at 500°C presented the lowest amount of open porosity of the three samples studied, which agreed well with the high value of relative density determined (i.e. 94% of the calculated value). Also, even if the sintering process started in this case from a mixture of U_3O_8 and UO_2, no particular morphology, such as columnar or equiaxed grains [57], was observed. For the samples sintered from powders converted at 800°C and 1000°C, a large amount of open porosity was then observed, again in good agreement with the density measurements. Moreover, the grains present at the surface of the pellets were found to keep the morphology inherited from the conversion process. In these conditions, the particles resulting from the so-called solarization step still possessed an angular aspect that slightly impact the microstructure of the pellet when comparing with samples of equivalent densities obtained from powders converted under reducing atmosphere.

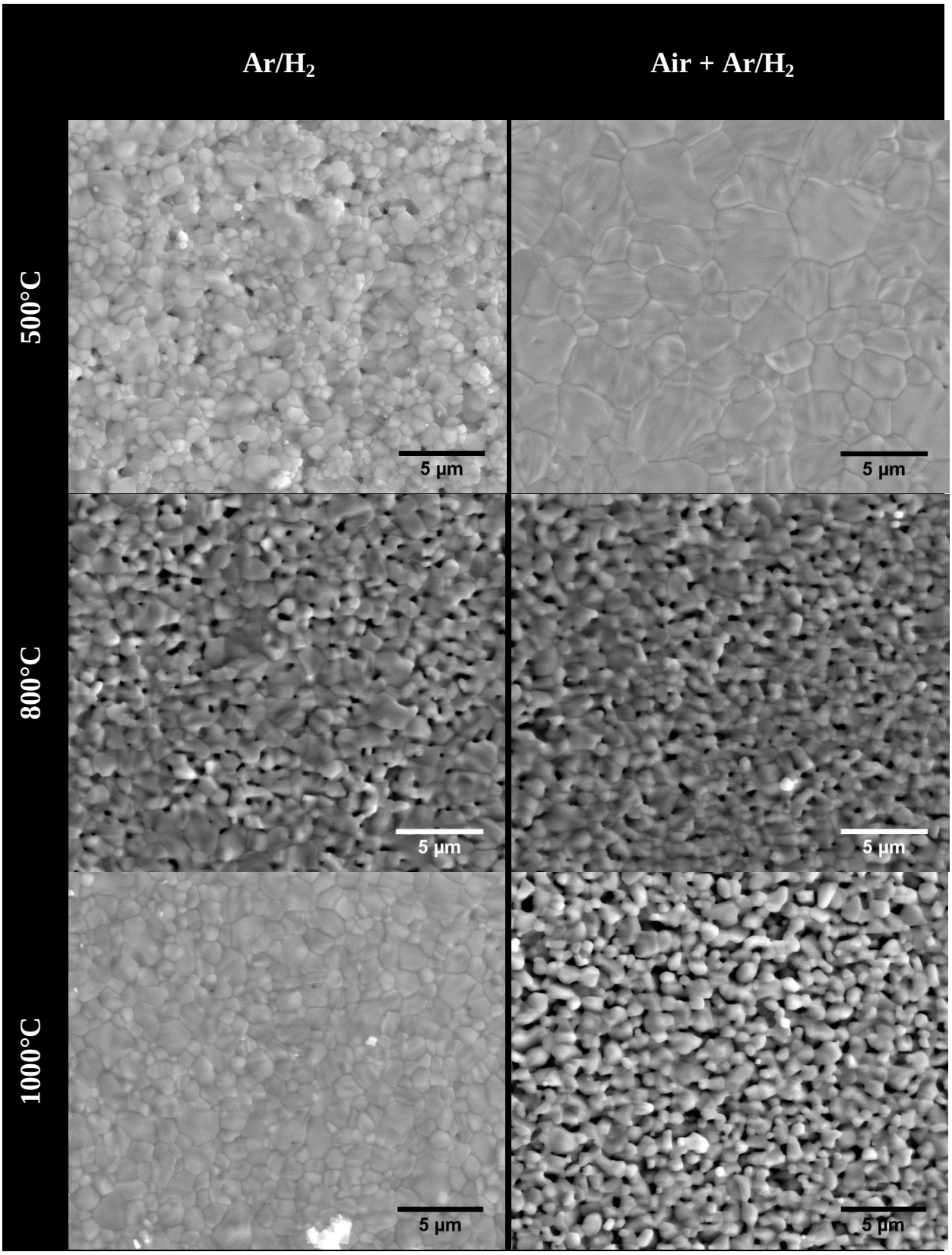

Figure 12. SEM micrographs of UO_2 sintered pellets obtained from differently converted powders.

4. Conclusion

The extensive characterization of the powders obtained from the conversion of oxalate precursor under various heating conditions revealed the crucial role played by the atmosphere of calcination. In the particular case of uranium-bearing compounds, the main differences evidenced arose from the oxidization of U(IV) under air. Indeed, this latter yields to modifications at the microscopic scale, particularly concerning diffusion coefficients that strongly affect the development of the powder microstructure. These changes not only concerned the crystallite size, which strongly increased during calcination under oxidizing atmosphere, but also the grains morphology at the macroscopic level through solarization-related processes. Finally, the densification processes as well as the final microstructure of the pellets prepared after sintering at high temperature also significantly differ regarding to the conditions of preparation of the starting powder. Such modifications mainly arise from the differences detailed above, but also from variations in the residual carbon content of the oxide powders.

Indeed, although expected from the data previously reported in the literature for other actinide-bearing oxides prepared from oxalate precursors, the effect of the atmosphere of conversion on the residual carbon content was confirmed in this study. As a matter of evidence, the amount of carbon was systematically found to be 4 to 5 times higher in the samples prepared under only reducing conditions. However, the residual carbon content appeared to be more likely a second-order parameter to be considered in order to assess the behaviour of the samples during the sintering process. Indeed, the more important variations stated when studying the microstructure of the sintered samples came from morphological or redox considerations (presence of U_3O_8 in the starting powder, decrease of reactivity through enhanced crystallite growth, …). Conversely, despite of the important differences measured in terms of carbon content in the final samples, neither the average grain size nor the relative density of the sintered pellets were found to be significantly modified, even if this latter appeared to be around 90%.

On this basis, the role of the carbon should be precised by performing sintering experiments at higher temperatures. Its exact nature and location within the UO_2 samples should be also investigated to better understand its behaviour under temperature and its influence on diffusion processes that control the sintering step.

Acknowledgements

Authors would like to thank J. Ravaux from ICSM for his help during SEM observations. J. Martinez specially thanks AREVA NC for funding his PhD work.

References

[1] J.E. Kelly, Generation IV International Forum: A decade of progress through international cooperation, *Progress in Nuclear Energy* 2014; **77**: 240-6.

[2] M.J. Bannister, W.J. Buykx, Sintering Mechanism in UO_{2+x}, *J Nucl Mater* 1977; **64**: 57-65.

[3] P. Dehaudt, L. Bourgeois, H. Chevrel, Activation energy of UO_2 and UO_{2+x} sintering, *J Nucl Mater* 2001; **299**: 250-9.

[4] A. Mohan, N.C. Soni, V.K. Moorthy, Sintering Diagrams of UO_2, *J Nucl Mater* 1979; **79**: 312-22.

[5] D. Lahiri, S.V.R. Rao, G.V.S.H. Rao, R.K. Srivastava, Study on sintering kinetics and activation energy of UO_2 pellets using three different methods, *J Nucl Mater* 2006; **357**: 88-96.

[6] M.S. Abdelazim, Contribution to Fuel-Element Fabrication of UO_2 Pellets Using Lower Sintering Temperatures, *J Nucl Mater* 1994; **217**: 217-9.

[7] C. Ganguly, U. Basak, Fabrication of High-Density UO_2 Fuel Pellets Involving Sol-Gel Microsphere Pelletization and Low-Temperature Sintering, *J Nucl Mater* 1991; **178**: 179-83.

[8] W. Timmermans, A. Vanheckhennen, F. Gorle, R. Debatist, Sintering Characterization of UO_2 Powders, *J Nucl Mater* 1978; **71**: 256-67.

[9] T.R.G. Kutty, P.V. Hegde, K.B. Khan, U. Basak, S.N. Pillai, A.K. Sengupta, G.C. Jain, S. Majumdar, H.S. Kamath, D.S.C. Purushotham, Densification behaviour of UO_2 in six different atmospheres, *J Nucl Mater* 2002; **305**: 159-68.

[10] M.C. Paraschiv, A. Paraschiv, V.V. Grecu, On the nuclear oxide fuel densification, swelling and thermal re-sintering, *J Nucl Mater* 2002; **302**: 109-24.

[11] B. Arab-Chapelet, S. Grandjean, G. Nowogrocki, F. Abraham, Synthesis of new mixed actinides oxalates as precursors of actinides oxide solid solutions, *J Alloy Compd* 2007; **444**: 387-90.

[12] B. Arab-Chapelet, S. Grandjean, G. Nowogrocki, F. Abraham, Synthesis and characterization of mixed An(IV)An(III) oxalates (An(IV) = Th, NP, U or Pu and An(III) = Pu or Am), *J Nucl Mater* 2008; **373**: 259-68.

[13] N. Hingant, N. Clavier, N. Dacheux, S. Hubert, N. Barre, R. Podor, L. Aranda, Preparation of morphology controlled $Th_{1-x}U_xO_2$ sintered pellets from low-temperature precursors, *Powder Technol* 2011; **208**: 454-60.

[14] B.J.F. Palmer, L.E. Bahen, A. Celli, Thoria-Urania Powders Prepared Via Bulk Microwave Denitration, *Am Ceram Soc Bull* 1984; **63**: 1030-4.

[15] K.C. Radford, R.J. Bratton, Properties, Blending and Homogenization of $(U,Th)O_2$-UO_2 Powder, *J Nucl Mater* 1975; **57**: 287-302.

[16] F. Abraham, B. Arab-Chapelet, M. Rivenet, C. Tamain, S. Grandjean, Actinide oxalates, solid state structures and applications, *Coord. Chem. Rev.* 2014; **266-267**: 28-68.

[17] S. Grandjean, B. Arab-Chapelet, A.C. Robisson, F. Abraham, P. Martin, J.P. Dancausse, N. Herlet, C. Leorier, Structure of mixed U(IV)-An(III) precursors synthesized by co-conversion methods (where An = Pu, Am or Cm), *J Nucl Mater* 2009; **385**: 204-7.

[18] C. Tamain, B.A. Chapelet, M. Rivenet, F. Abraham, R. Caraballo, S. Grandjean, Crystal Growth and First Crystallographic Characterization of Mixed Uranium(IV)-Plutonium(III) Oxalates, *Inorg Chem* 2013; **52**: 4941-9.

[19] D. Dollimore, The Thermal-Decomposition of Oxalates - a Review, *Thermochim Acta* 1987; **117**: 331-63.

[20] N. Vigier, S. Grandjean, B. Arab-Chapelet, F. Abraham, Reaction mechanisms of the thermal conversion of Pu(IV) oxalate into plutonium oxide, *J Alloy Compd* 2007; **444**: 594-7.

[21] N. Clavier, N. Hingant, M. Rivenet, S. Obbade, N. Dacheux, N. Barre, F. Abraham, X-Ray Diffraction and mu-Raman Investigation of the Monoclinic-Orthorhombic Phase Transition in $Th_{1-x}U_x(C_2O_4)_2.2H_2O$ Solid Solutions, *Inorg Chem* 2010; **49**: 1921-31.

[22] L. Duvieubourg-Garea, N. Vigier, F. Abraham, S. Grandjean, Adaptable coordination of U(IV) in the 2D-(4,4) uranium oxalate network: From 8 to 10 coordinations in the uranium (IV) oxalate hydrates, *J Solid State Chem* 2008; **181**: 1899-908.

[23] G.D. White, L.A. Bray, P.E. Hart, Optimization of Thorium Oxalate Precipitation Conditions Relative to Derived Oxide Sinterability, *J Nucl Mater* 1981; **96**: 305-13.

[24] P. Balakrishna, B.P. Varma, T.S. Krishnan, T.R.R. Mohan, P. Ramakrishnan, Thorium-Oxide - Calcination, Compaction and Sintering, *J Nucl Mater* 1988; **160**: 88-94.

[25] A. Jain, K. Ananthasivan, S. Anthonysamy, P.R.V. Rao, Synthesis and sintering of $(U_{0.72}Ce_{0.28})O_2$ solid solution, *J Nucl Mater* 2005; **345**: 245-53.

[26] Y. Altas, M. Eral, H. Tel, Preparation of homogeneous $(Th_{0.8}U_{0.2})O_2$ pellets via coprecipitation of $(Th,U)(C_2O_4)_2.nH_2O$ powders, *J Nucl Mater* 1997; **249**: 46-51.

[27] Y. Harada, UO_2 sintering in controlled oxygen atmospheres of three-stage process, *J Nucl Mater* 1997; **245**: 217-23.

[28] X.D. Yang, J.C. Gao, Y. Wang, X. Chang, Low-temperature sintering process for UO_2 pellets in partially-oxidative atmosphere, *T Nonferr Metal Soc* 2008; **18**: 171-7.

[29] N. Dacheux, V. Brandel, M. Genet, Synthesis and Properties of Uranium Chloride Phosphate Tetrahydrate - $UClPO_4.4H_2O$, *New J Chem* 1995; **19**: 1029-36.

[30] N. Dacheux, V. Brandel, M. Genet, Synthesis and Characterization of Mixed-Valence Uranium Orthophosphate - $U(UO_2)(PO_4)_2$, *New J Chem* 1995; **19**: 15-25.

[31] P. Thompson, D.E. Cox, J.B. Hastings, Rietveld refinement of Debye-Scherrer synchrotron X-ray data from Al_2O_3, *Journal of Applied Crystallography* 1987; **20**: 79-83.

[32] C. Frontera, J. Rodriguez-Carvajal, FullProf as a new tool for flipping ratio analysis, *Physica B: Condensed Matter* 2003; **335**: 219-22.

[33] S. Dash, R. Krishnan, M. Kamruddin, A.K. Tyagi, B. Raj, Temperature programmed decomposition of thorium oxalate hexahydrate, *J Nucl Mater* 2001; **295**: 281-9.

[34] D.S. Bharadwaj, A.R.V. Murthy, Studies on Thermal Behaviour of Uranium (IV) Oxalate, *Indian J Chem* 1964; **2**: 391-&.

[35] N. Hingant, N. Clavier, N. Dacheux, N. Barre, S. Hubert, S. Obbade, F. Taborda, F. Abraham, Preparation, sintering and leaching of optimized uranium thorium dioxides, *Journal of Nuclear Materials* 2009; **385**: 400-6.

[36] L. De Almeida, S. Grandjean, N. Vigier, F. Patisson, Insights into the Thermal Decomposition of Lanthanide(III) and Actinide(III) Oxalates - from Neodymium and Cerium to Plutonium, *Eur J Inorg Chem* 2012; **31**: 4986-99.

[37] I. Amato, R.L. Colombo, The Influence of Organic Additions on the Solarization and Grain Growth of Sintered UO_2, *J Nucl Mater* 1964; **11**: 348-51.

[38] V. Tyrpekl, C. Berkmann, M. Holzhauser, F. Kopp, M. Cologna, T. Wangle, J. Somers, Implementation of a spark plasma sintering facility in a hermetic glovebox for compaction of toxic, radiotoxic, and air sensitive materials, *Rev Sci Instrum* 2015; **86**.

[39] K. Asakura, K. Takeuchi, Effect of residual carbon on the sintering behavior of MOX pellets, *J Nucl Mater* 2006; **348**: 165-73.

[40] S. Gosse, C. Gueneau, T. Alpettaz, S. Chatain, C. Chatillon, F. Le Guyadec, Kinetic study of the UO_2/C interaction by high-temperature mass spectrometry, *Nucl Eng Des* 2008; **238**: 2866-76.

[41] E. Oktay, A. Yayli, Physical properties of thorium oxalate powders and their influence on the thermal decomposition, *J Nucl Mater* 2001; **288**: 76-82.

[42] S. Hubert, J. Purans, G. Heisbourg, P. Moisy, N. Dacheux, Local structure of actinide dioxide solid solutions $Th_{1-x}U_xO_2$ and $Th_{1-x}Pu_xO_2$, *Inorg Chem* 2006; **45**: 3887-94.

[43] B.O. Loopstra, Phase Transition in Alpha-U_3O_8 at 210°C, *J Appl Crystallogr* 1970; **3**: 94-&.

[44] W.H. Zachariasen, Crystal Chemical Studies of the 5f-Series of Elements .1. New Structure Types, *Acta Crystallogr* 1948; **1**: 265-9.

[45] H.R. Hoekstra, S. Siegel, L.H. Fuchs, J.J. Katz, The Uranium-Oxygen System - $UO_{2.5}$ to U_3O_8, *J Phys Chem-Us* 1955; **59**: 136-8.

[46] H. Assmann, W. Dorr, M. Peehs, Control of UO_2 Microstructure by Oxidative Sintering, *J Nucl Mater* 1986; **140**: 1-6.

[47] D.G. Leme, H. Matzke, The Diffusion of Uranium in U_3O_8, *J Nucl Mater* 1983; **115**: 350-3.

[48] H. Matzke, On Uranium Self-Diffusion in UO_2 and UO_{2+x}, *J Nucl Mater* 1969; **30**: 26-&.

[49] K.W. Song, K.S. Kim, K.W. Kang, Y.H. Jung, Grain size control Of UO_2 pellets by adding heat-treated U_3O_8 particles to UO_2 powder, *J Nucl Mater* 2003; **317**: 204-11.

[50] I. Amato, R.L. Colombo, A.M. Protti, On a Case of Solarization during Steam Sintering of UO_2 Pellets, *J Nucl Mater* 1963; **8**: 271-2.

[51] I. Amato, R.L. Colombo, A.M. Protti, Pore Growth during Solarization of Sintered UO_2, *J Nucl Mater* 1964; **13**: 265-7.

[52] L. Claparede, N. Clavier, N. Dacheux, A. Mesbah, J. Martinez, S. Szenknect, P. Moisy, Multiparametric Dissolution of Thorium-Cerium Dioxide Solid Solutions, *Inorg Chem* 2011; **50**: 11702-14.

[53] L. Claparede, N. Clavier, N. Dacheux, P. Moisy, R. Podor, J. Ravaux, Influence of Crystallization State and Microstructure on the Chemical Durability of Cerium-Neodymium Mixed Oxides, *Inorg Chem* 2011; **50**: 9059-72.

[54] D. Horlait, F. Lebreton, T. Delahaye, P. Blanchart, Dilatometric Study of $U_{1-x}Am_xO_{2\pm\delta}$ Sintering: Determination of Activation Energy, *J Am Ceram Soc* 2013; **96**: 3410-6.

[55] E.B. Slamovich, F.F. Lange, Densification Behavior of Single-Crystal and Polycrystalline Spherical-Particles of Zirconia, *J Am Ceram Soc* 1990; **73**: 3368-75.

[56] J. Martinez, N. Clavier, A. Mesbah, F. Audubert, X.F. Le Goff, N. Vigier, N. Dacheux, An Original Precipitation Route toward the Preparation and the Sintering of Highly Reactive Uranium Cerium Dioxide Powders, *J Nucl Mater* 2015; **462**: 173-81.

[57] J.H. Yang, Y.W. Rhee, K.W. Kang, K.S. Kim, K.W. Song, S.J. Lee, Formation of columnar and equiaxed grains by the reduction of U_3O_8 pellets to UO_{2+x}, *J Nucl Mater* 2007; **360**: 208-13.